

New Approach to Non-Volatile Metal Ion Production Using Plasma Ion Source with Internal Evaporator

Marcin Turek¹, Andrzej Drożdżel¹, Krzysztof Pyszniak¹,
Janusz Filiks^{1*}, Paweł Węgierek²

¹ Institute of Physics, Maria Curie-Skłodowska University in Lublin, pl. M. Curie-Skłodowskiej 1, 20-031 Lublin, Poland

² Faculty of Electrical Engineering and Computer Science, Lublin University of Technology, Nadbystrzycka 38A, 20-618 Lublin, Poland

* Corresponding author's e-mail: janusz.filiks@mail.umcs.pl

ABSTRACT

A new approach to application the internal evaporator in an arc discharge ion source is presented, namely a crucible with a plug made of feeding substance. This solution is suitable especially for high-melting point metallic feeding substances. The ion source was tested using Ni and Cr. Basic ion source characteristics, i.e. dependences of ion current and discharge voltage on discharge and filament currents as well as on the external magnetic field flux density are shown and discussed in order to find optimal working conditions. The maximal ion currents were 18 μA for Ni^+ and 38 μA for Cr^+ . The stability of the ion current was also tested. It was proven that ion source is able to provide intense ion beam current long enough to perform irradiations with the fluence of $\sim 5 \times 10^{15} \text{ cm}^{-2}$ confirming the usefulness of the design for ion implantation purposes.

Keywords: ion sources, ion implantation, ion beams.

INTRODUCTION

Over several decades ion implantation technique has become a very popular tool for modification of physical and chemical properties of semiconductors [1–3] (actually, ion implantation is one of cornerstones of semiconductor industry), metals [4, 5] and polymers [6, 7] as well as production of new materials [8]. As there is a wide variety of technological processes involving different dopants, fluences and flux densities different solutions are developed based on a multitude of ion sources [9, 10], which are a crucial for obtaining good quality high intensity ion beams.

Implantation of transition metals like Cr or Ni could be used for enhancing the corrosion resistance of metals and alloys [11–13] as well as for improvement of their tribological [14], fatigue [15] and erosive [16] properties. It was also shown that formation of intermetallic Laves

phases in titanium and ZrNb alloy is possible via Cr^+ ion implantation [17, 18]. Irradiation with Cr^+ ions can also change magnetic properties of semiconductors like InGaN or CdTe [19, 20] as well as minerals like rutile [21]. It was also shown that Ni^+ implantation followed by annealing leads to formation of magnetic nanoparticles e.g. in silicon [22], SiO_2 [23] or ZnO [24]. A similar combination of Ni^+ implantation and annealing enables change of optical properties of sapphire [25]. Implantation of Ni^+ was also used to modify structural, physical and chemical properties of polymers [26–28]

One of the most useful method for high melting point metal ion beams is using the MEVVA (MEtal Vapor Vacuum Arc) ion sources [29, 30]. Another effective and widely used method is MIVOC (MEtal-Ions-from-VOLatile-Compounds) employing volatile (usually organic) compounds supplied as a feeding gas to the

electron cyclotron ion source [31–34]. The other methods that should be also mentioned here are: plasma sputtering [35, 36], laser ablation [37] also in the version combined with electron cyclotron resonance [38] or electron beam ionisation [39].

Arc discharge ion source with cylindrical anode and an internal evaporator was developed in Institute of Physics in Lublin ten years ago. It was initially dedicated for production of rare earth's and aluminum ions [40, 41], but soon proved its effectiveness for a variety of other ions becoming almost universal solution used for ion implantation purposes in Lublin [42, 43]. The versatility of that particular kind of ion sources is due to the possibility of tailoring of the internal evaporator, namely size and placement inside the source [44]. It should be also mentioned here that ion source could be feed with chlorine and fluorine containing working gases like CCl_4 , HCCl_3 or CCl_2F_2 which proved to work well for production of Mo^+ and Ta^+ ions [45, 46] as well as rare earths' ions using their oxides [47].

The arc discharge ion source in its standard version (i.e. with an internal evaporator filled with small metal lumps as feeding substance) provided a moderate current of $\sim 10 \mu\text{A}$ (Cr^+ ions) and $40 \mu\text{A}$ (Ni^+ ions). The current was, however, unstable and decreased rapidly with time as the feeding substance near the evaporator tips was spent. This effect was mostly due to the fact that relatively large power (both of the arc discharge and delivered to the cathode filament) was required to provide high enough pressure of feeding substance vapors, as the melting points of considered substances are rather high ($1455 \text{ }^\circ\text{C}$ for Ni and $1907 \text{ }^\circ\text{C}$ for Cr). To summarize up, total achievable fluences were much below 10^{15} cm^{-2} within the single working cycle. Some test with hydrated chlorides of Ni and Cr were performed, but the achieved currents were not satisfactory. Moreover, in the case of chromium chloride a very broad and intense peak covering the masses 51 and 52 was observed, coming most probably from some molecular ions containing Cl (HClO seems to be a probable explanation).

The current paper presents a new approach to production of Cr^+ and Ni^+ ions with an internal evaporator placed inside the discharge region. This time feeding substance has a form of relative large plug/screw that has direct contact with the discharge plasma. The paper contains brief description of the ion source as well as experimental setup. Some basic working characteristics of

the ion source are shown and discussed in order to find optimal conditions for possibly large ion beam production. These characteristics are: dependences of extracted ion current and discharge voltage on the discharge and filament currents on the magnetic field flux density imposed by a surrounding electromagnet. Moreover, dependence of the ion current on time/cumulated fluence is presented and commented.

EXPERIMENTAL

The ion source used for Ni^+ and Cr^+ ion beam production was the arc discharge ion source with cylindrical anode, described in previous papers [40–44]. Its cross-sectional view is shown in Figure 1.

Both the anode and cathode filament mounts (that form the discharge chamber) are made of molybdenum, although any other refractive metal could be used. The anode and filament mounts are separated by cylindrical insulators made of boron nitride. The discharge chamber has the internal diameter of $\sim 11 \text{ mm}$ and the length of $\sim 20 \text{ mm}$. A spiral cathode filament is made of tungsten wire of 0.75 mm in diameter and has typically 6–7 coils. The hot filament is the source of primary electrons that ignite and maintain the discharge in the region between cathode and anode. The filament is heated by the filament current I_c reaching 40 A . The discharge current I_a may be set up to 4.5 A (note that electrical connections of the ion source are shown in Figure 2). The arc discharge is ignited by setting the anode voltage U_a to approximately 100 V and then increasing the filament current (and consequently the amount of primary electrons) until the discharge burns. After a short period of time the discharge voltage U_a stabilizes at much lower values ($20\text{--}40 \text{ V}$ depending on the ionized substance). It should be mentioned here that the ion source chamber is placed inside the electromagnet coil. The purpose of the external magnetic field is to partially compensate the strong magnetic field from the spiral cathode as well as to shift the discharge plasma as close as possible to the extraction region in order to improve performance.

The feeding substance is usually placed inside the evaporator closed by threaded plug/screw. The crucible/evaporator is heated to very high temperatures by both the filament and the discharge plasma, and the vapors of feeding

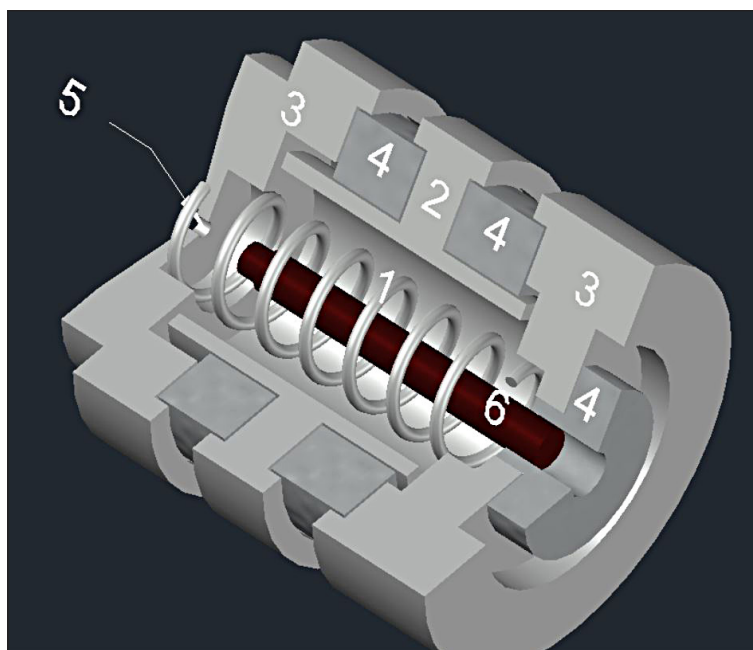


Fig. 1. Cross-section of the ion source: 1 – spiral cathode filament, 2 – anode, 3 – cathode filament mounts. 4 – insulators, 5 – extraction opening, 6 – evaporator

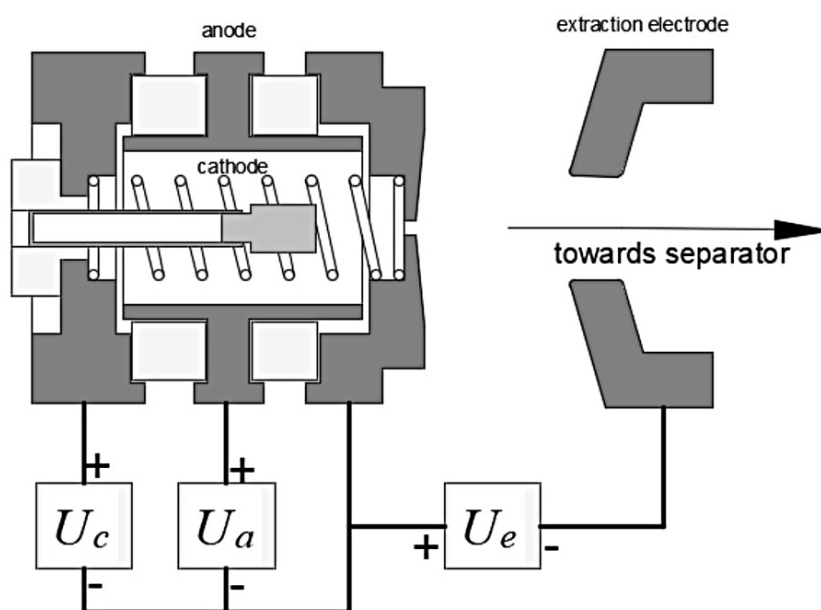


Fig. 2. The scheme of electrical connections of the ion source and extraction electrode

substance reach directly the discharge region, where they are ionized by electrons. Such a solution work especially well for substance characterized by high vapor pressure and low melting point. However, placing lumps of the high melting point metal like Cr inside the evaporator results in a mediocre beam current for a limited time – namely until the Cr lumps close to the crucible tip are melt and evaporated. On the other hand, placing the metal lumps or powder directly inside the chamber is not a good solution – the

short circuit of anode an cathode is inevitable. As it was already mentioned earlier a variety of evaporators was used with the considered ion source, varying in length and weight. For our purposes we decide to use relatively small (length of ~2 cm, see Figure 3) evaporator made of molybdenum. It should be noted that the plug is made of the feeding material (Cr or Ni in the considered case). Such approach guarantees high enough vapor pressure as the feeding material is in contact with the discharge plasma. The feeding material

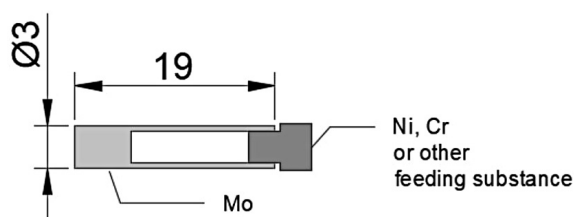


Fig. 3. The schematic view of the evaporator

could be also put inside the crucible (in the form of lump, powder or even a rod) in order to extend the working cycle of the ion source after the plug/screw is evaporated.

The ions produced in the discharge are pulled out through the extraction orifice of the diameter ~ 1 mm due to the extraction voltage $V_{ext} = 25$ kV. The ion beam is then formed using a lens triplet. The initial beam reaches a 90° sector field separating electromagnet. The obtained mass-separated beam is accelerated using the final additional voltage $V_{acc} = 75$ keV. The mass separated ion currents can be measured using a retractable Faraday cup placed behind the acceleration tube. It should be mentioned here that the sample chamber itself is a kind of Faraday cup that enables measurements of the ion current at the target, when the beam sweeping system is active.

RESULTS

Characteristics of the ion source were determined as soon as the ion source works stable i.e. approximately 20 minutes after the discharge was ignited. In order to find the optimal working conditions characteristics of the ion source were measured, including dependences of ion current and discharge voltage on the discharge voltage I_a , filament current I_c as well as on the magnetic induction B .

Figure 4 shows the dependences of the mass-separated ion currents of Ni^+ and Cr^+ on the discharge current I_a , measured when the other working parameters (like filament current I_c and magnetic induction B) were constant. In both cases the feeding substance had a form of a plug in the evaporator. For both substances increase of I_{ion} with I_a was observed. This was due to the rising crucible temperature as well as electronic density and, consequently, ionization probability. The rise of $I_{ion}(I_a)$ curve was followed by the saturation which was observed for $\sim I_a = 1$ A for Cr and for higher values of discharge current ($I_a = 3$ A) in

the case of Ni. This saturation may be caused by mostly by the decreasing discharge voltage (and consequently, electron energy) with I_a , which leads to less probable ionization by impinging electrons, as the rule-of-a-thumb says that optimal U_a should be 3–4 larger than the ionization potential. It should be noticed that in both cases the saturation takes place when U_a falls below 40 V. Another reasons could be the increasing ion recombination probability as well as screening of the extraction field when the plasma density is growing. Maximal ion currents are $38 \mu\text{A}$ and $18 \mu\text{A}$ for Cr^+ and Ni^+ , respectively.

Figure 5 presents dependences of I_a and U_a on the filament current I_c . A typical behavior (that was previously observed in most cases [40–44]) was also seen for Ni: the I_{ion} current initially grows with I_c up to certain value (due to the increasing electronic density and vapor pressure – as the filament and crucible become more and more hot), then a decrease of ion current is observed.

This degradation of ion source performance could due to the fact that the U_a and, as it was mentioned previously, electron energy decrease with rising plasma density. One should have in mind that electron impact ionization cross-section dependences on energy have maxima for several electronvolts. Therefore, $U_a(I_c)$ and $I_{ion}(I_c)$ are closely related to the behavior of the dependence of electron impact ionization cross-section σ on the electron energy E . It is especially well visible if we transform $U_a(I_c)$ and $I_{ion}(I_c)$ into $I_{ion}(U_a)$ as in Figure 6.

In the case of Ni the shape of $I_{ion}(U_a)$ closely resembles the typical trend of typical $\sigma(E)$ dependence. The dependences of $U_a(I_c)$ and $I_{ion}(I_c)$ characteristics for Cr^+ could be understood in the same way, but one deals with the descending part of the corresponding $\sigma(E)$ curve. This is due to the fact that characteristics for Cr^+ were measured for smaller discharge current (0.7 A) and the decrease of the extracted ion current would require much higher filament currents. Maximal ion currents are achieved for approximately 50 V (Ni^+) and 20 V (Cr^+).

The third pair of considered characteristics are the dependences of I_a and U_a on magnetic induction. They are shown in Figure 7.

The magnetic induction was measured using the LakeShore model 450 gaussmeter. In both cases rather high B values were required (near 12 mT). This is different than most of results obtained in previous papers with closed

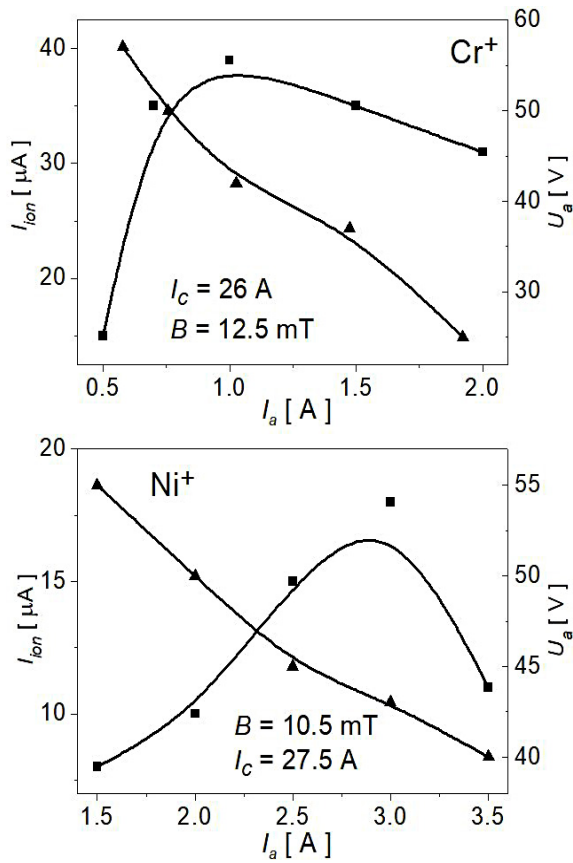


Fig. 4. Dependences of Ion (squares) and U_a (triangles) on the discharge current

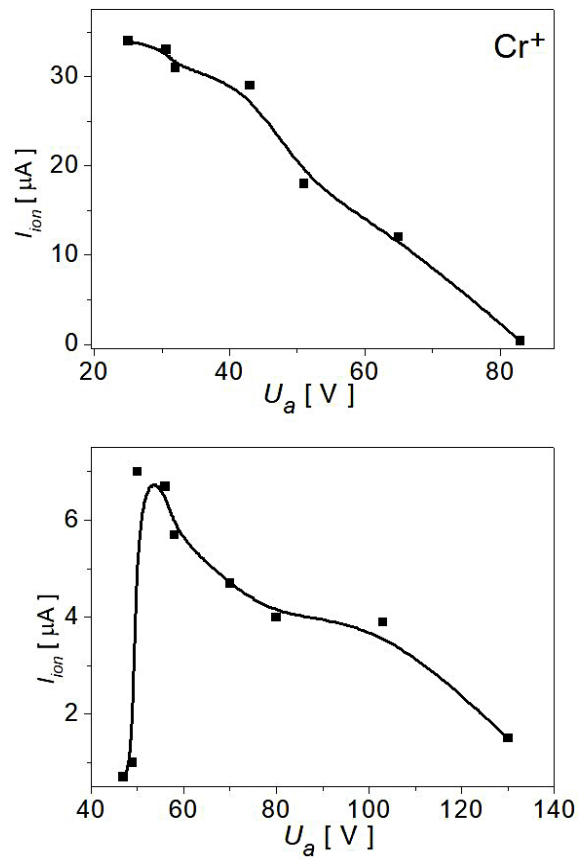


Fig. 6. Dependences of the ion current on discharge voltage U_a

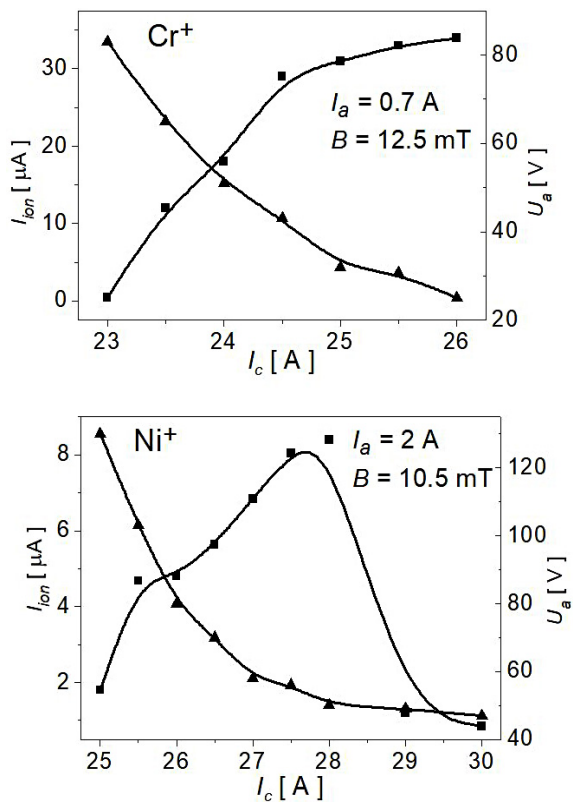


Fig. 5. Dependences of I_{ion} (squares) and U_a (triangles) on the filament current

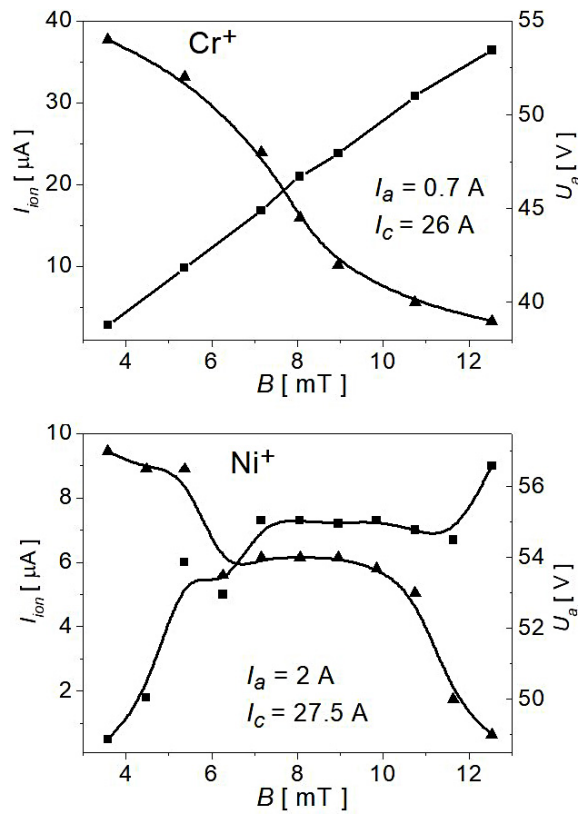


Fig. 7. Dependences of I_{ion} (squares) and U_a (triangles) on the external magnetic induction

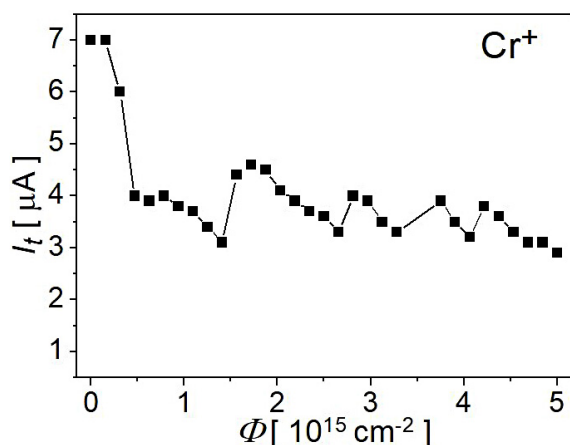


Fig. 8. Ion current (Cr^+) measured on the target as a function of fluence

evaporator, when a maximum for intermediate B values (near 7 mT) was observed. Such B value was required to compensate the magnetic field from the spiral cathode. In the considered case of Ni and Cr plugs the strong magnetic field is needed to push the discharge plasma near the extraction opening and enhance ion source performance. One can see that the ion current increases smoothly (the case of Cr) or less smoothly (for Ni there is a broad plateau in the range from 7 mT up to 11 mT) with the magnetic flux density, or, in other words, with the current in the external electromagnet. As in the case of the dependences on the discharge current the increase of B leads to the reduction of discharge voltage.

Figure 8 shows the evolution of the ion current at the target (when the beam sweeping system of the implanter is active) as a function of the implantation fluence (instead of time).

One can see that the ion current is rather fast reduced to 60% of initial value, but after that the ion current remains on the same level. Of course some corrections of working parameters are needed (like slight increases of discharge current and reduction of the filament current in order to keep the discharge voltage in its optimal range) and there are visible signs of these actions – temporary increases of the ion current. These corrections are necessary as the feeding substance near the plasma melts and evaporates during the ion source operation and the evaporator temperature needs to be increased. The presented irradiation with the fluence $5 \times 10^{15} \text{ cm}^{-2}$ was performed within approximately 1.5 hour.

CONCLUSIONS

A new solution enabling production of ions of high-melting point metals using an arc discharge ion source with semi-opened evaporator. The ion source was tested using Cr and Ni as feeding materials, although the presented approach seems to be applicable to other refractory metals. Some chosen basic working characteristics of the ion source were presented and discussed in the paper in order to find optimal conditions for effective ion beam production. It was found that typical currents 18 μA and 38 μA were achieved for Ni^+ and Cr^+ , respectively. Optimal discharge voltage should be kept in the range 20–50 V. In the tested cases $I_a = 2 \text{ A}$ is a good choice, although the discharge current has to be increased during ion source operation in order to increase temperature of the parts of the evaporator that are farther from the discharge region. The stability of the ion source was tested for ~ 100 minutes, which is a fair result for the internal evaporator based ion source. The presented approach enables Ni^+ or Cr^+ implantations with fluences $5 \times 10^{15} \text{ cm}^{-2}$ within a single working cycle of the implanter.

Acknowledgements

The publication of the paper is supported by the “Excellence in Science” program of the Polish Ministry of Education and Science (Międzynarodowa Konferencja “Implantacja jonowa i inne zastosowania jonów i elektronów ION’2020”)

REFERENCES

- Milosevic M.M., Chen X., Yu X., Dinsdale N.J., Aktas O., Oo S.Z., Khokhar A.Z., et al. Ion Implantation of Germanium Into Silicon for Critical Coupling Control of Racetrack Resonators. *Journal of Lightwave Technology*. 2020; 38(7): 1865–1873.
- Miskiewicz S.A., Komarov A.F., Komarov F.F., Soroka S.A. Radiation Degradation of Bipolar Transistor Current Gain, *Acta Physica Polonica A*. 2017; 132(2): 288–290.
- Komarov F., Vlasukova L., Milchanin O., Mudryi A., Dunets B., Wesch W., Wendler E. Structure and optical properties of silicon layers with GaSb nanocrystals created by ion-beam synthesis. *Phys. Status Solidi A*. 2012; 209(1): 148–152.
- Somasundaram S., Ionescu M., Kannan Mathan B. Ion Implantation of Calcium and Zinc in Mag-

- nesium for Biodegradable Implant Applications. *Metals*. 2018; 8(1): 30.
5. Kamiński M., Budzyński P., Szala M., Turek M. Comparing of Microhardness of the Stellite 6 Cobalt Alloy Implanted with 175 keV Mn⁺ Ions and 120 keV N⁺ Ions *Adv. Sci. Technol. Res. J.* 2019; 13(3): 179–185.
 6. Kosinska A., Jagielski J., Ostaszewska U., Wyszowska E., Clozel M., Kurpaska L., Romaniec M. Functional properties of low energy ion-irradiated acrylonitrile-butadiene rubber. *Nucl. Instr. Meth. B.* 2019; 443: 15–18.
 7. Sagheer R., Shahid Rafique M., Saleemi F., Arif S., Naab F., Toader O., Mahmood A.D., Rashid R., Hussain I. Modification in surface properties of poly-allyl-diglycol-carbonate (CR-39) implanted by Au⁺ ions at different fluences. *Materials Science-Poland*. 2016; 34(2): 468–478.
 8. Prucnal S., Žuk J., Hübner R., Duan J., Wang M., Pysznik K., Drozdziel A., Turek M., and Zhou S., Electron Concentration Limit in Ge Doped by Ion Implantation and Flash Lamp Annealing. *Materials*. 2020; 13(6): 1408.
 9. Brown I.G. *The Physics and Technology of Ion Sources*. Wiley, 2004.
 10. Zhang H., *Ion Sources*. Science Press and Springer Verlag, 1999.
 11. Rangel C.M., Paiva T.I.C. Chromium ion implantation for inhibition of corrosion of aluminium. *Surface and Coatings Technology*. 1996; 83(1-3): 194–200.
 12. Dai J., Liu Z., Yu B., Ruan Q., Chu P.K. Effects of Ti, Ni, and Dual Ti/Ni Plasma Immersion Ion Implantation on the Corrosion and Wear Properties of Magnesium Alloy. *Coatings*. 2020; 10(4): 313.
 13. Tian L.P., Zhao X.H., Zuo Y. Formation of Anti-corrosion Clusters on Anodic Alumina Films by Ni Ion Implantation. *Advanced Materials Research*. 2006; 11–12: 89–94.
 14. Onate J.I., Alonso F., Garcia A. Improvement of tribological properties by ion implantation. *Thin Solid Films*. 1998; 317(1–2): 471–476.
 15. Chen X., Soveja A., Chaussimier M., Zhang P., Wei D., Ding F. Effect of MEVVA ion implantation on fatigue properties of TC18 titanium alloy. *Surface and Coatings Technology*. 2018; 344: 572–578.
 16. Szala M., Chocyk D., Skic A., Kamiński M., Macek W., Turek M. Effect of Nitrogen Ion Implantation on the Cavitation Erosion Resistance and Cobalt-Based Solid Solution Phase Transformations of HIPed Stellite 6. *Materials*. 2021; 14(9): 2324.
 17. Prudencio LM., Paramês L., Conde O., da Silva R.C. Cr ion implantation into Ti: Part I. Formation of intermetallic Laves phase, *Surface and Coatings Technology*. 2006; 200(12–13): 3907–3912.
 18. Ryabchikov A.I., Kashkarov E.B., Shevelev A.E., Syrtanov M.S. High-intensity chromium ion implantation into Zr-1Nb alloy. *Surface and Coatings Technology*. 2020; 383: 125272.
 19. Wang Z., Wu H., Liu Y., Liu C. Room Temperature Ferromagnetism in InGaN Nanostructures Induced by Cr⁺ ion Implantation. *Nanomaterials*. 2020; 10(6): 1128.
 20. Popovych V.D., Böttger R., Heller R., Zhou S., Bester M., Cieniek B., Mroccka R., Lopucki R., Sagan P., Kuzma M. Heavy doping of CdTe single crystals by Cr ion implantation. *Nucl. Instr. and Meth. B.* 2018; 419: 26–31.
 21. Ding B.F. Investigation of structural and magnetic properties of Ni implanted rutile. *Science China Physics, Mechanics and Astronomy*. 2012; 55: 247–251.
 22. Sundaravel B., Kalavathi S., Santhana Raman P., Satyam P. V., Nair K.G.M. Formation of NiSi₂ nanoclusters by Ni ion implantation into Si(100) and the effect of preinjection of Si²⁺ ions, *AIP Conference Proceedings*. 2012; 1447: 285–286.
 23. Prakash T., Williams G., Kennedy J. Synthesis of magnetic nanoparticles by low-energy dual ion implantation of iron and nickel into silicon dioxide followed by electron beam annealing. *International Journal of Nanotechnology*. 2017; 14(1–6): 348–355.
 24. Zhou S., Potzger K., von Borany J., Grötzschel R., Skorupa W., Helm M., Fassbender J. Crystallographically oriented Co and Ni nanocrystals inside ZnO formed by ion implantation and postannealing. *Phys. Rev. B*. 2008; 77: 035209.
 25. Xiang X., Zu X.T., Bao J.W., Zhu S., Wang L.M. Optical properties and structure characterization of sapphire after Ni ion implantation and annealing. *Journal of Applied Physics*. 2005; 98: 073524
 26. Sze J.Y., Tay B.K., Pakes C.I., Jamieson D.N., Praver S. Conducting Ni nanoparticles in an ion-modified polymer. *Journal of Applied Physics*. 2005; 98: 066101.
 27. Nathawat R., Vijay Y.K., Kumar P., Kulriya P., Ganesan V., Sathe V. Physically and Chemically Modified Polycarbonate by Metal Ion Implantation. *Advances in Polymer Technology*. 2008; 27(3): 143–151.
 28. Popok V. Ion implantation of polymers: Formation of nanoparticulate materials. *Rev. Adv. Mater. Sci.* 2012; 30: 1–26.
 29. Brown I.G., Feinberg B., Galvin J.E. Multiply stripped ion generation in the metal vapor vacuum arc. *J. Appl. Phys.* 1988; 63: 4889.
 30. Gao Y., Yu Y.J., Tang D.L., Huang Y.M., Geng M., Gong X.R. Development and experiments of

- a MEVVA ion source. *Rev. Sci. Instr.* 1994; 65(4): 1281.
31. Koivisto H., Arje J., Nurmia M. Metal ions from the volatile compounds method for the production of metal ion beams. *Rev. Sci. Instr.* 1998; 69(2): 785.
 32. Bogomolov S.L., Bondarchenko A.E., Efremov A.A., Kuzmenkov K.I., Lebedev A.N., Lebedev K.V., Lebedev V.Y., Loginov V.N., Mironov V.E., Yazvitsky N.Y. Production of intense metal ion beams from ECR ion sources using the MIVOC method. *Physics of Particles and Nuclei Letters.* 2015; 12(7): 824–830.
 33. Jovović J., Cvetić J., Dobrosavljević A., Nedeljković T., Jovanović B., Draganić I. MIVOC method at the mVINIS ion source. *Nuclear Technology and Radiation Protection.* 2007; 22(2): 10–14.
 34. Kheswa N., Thomae R., Nemulodi F., Mira J., Conradie L., Fourie D., Bogomolov S., Efremov A. Production of high intensity nickel-ion beams with high isotope purity with the metal ions from volatile compound (MIVOC) method, *AIP Conf. Proc.* 2018; 2011: 040007.
 35. Kanter M. High-current sputtering ion source for refractory metals, *Nucl. Instrum. Meth. B.* 1992; 70(1–4): 200–204.
 36. Oks E., Anders A. A self-sputtering ion source: A new approach to quiescent metal ion beams. *Rev. Sci. Instr.* 2010; 81(2): 02B306.
 37. Gill C.G., Garrett A.W., Hemberger P.H., Nogar N.S. Resonant laser ablation as a selective metal ion source for gas-phase ion molecule reactions. *J Am Soc Mass Spectrom.* 1996; 7(7): 664–667.
 38. Gammino S., Torrisi L., Ciavola G., Ando L., Wolowski J., Laska L., Krasa J., Picciotto A. Highly charged heavy ion generation by pulsed laser irradiation. *Nucl. Instrum. Meth. B.* 2003; 209(2): 345–350.
 39. Nitschke J. M. An electron-beam-generated-plasma ion source for on-line isotope separation. *Nucl. Instrum. Meth. A* 1985; 236(1): 1–16.
 40. Turek M., Prucnal S., Drożdźiel A., Pyszniak K. Arc discharge ion source for europium and other refractory metals implantation. *Rev. Sci. Instr.* 2009; 80(4): 043304.
 41. Turek M., Drożdźiel A., Pyszniak K., Prucnal S., Zuk J. Źródło jonów z parownikiem ogrzewanym przez wyładowanie łukowe. Symulacje komputerowe i eksperyment. *Przegląd Elektrotechniczny.* 2010; 86(7): 193–196. (in Polish)
 42. Turek M., Drożdźiel A., Pyszniak K., Prucnal S. Versatile plasma ion source with an internal evaporator, *Nucl. Instr. Meth. B.* 2011; 269, 700–707.
 43. Turek M., Drożdźiel A., Pyszniak K., Prucnal S., Mączka D., Yushkevich Yu., Vaganov, Yu. Plasma Sources of Ions of Solids. *Instrum. Exp. Techn.* 2012; 55; 469–481.
 44. Turek M., Drożdźiel A., Pyszniak K., Prucnal S. Tailoring the Internal Evaporator for Effective Ion Beam Production. Volatile vs. Non-Volatile Substances. *Acta Physica Polonica A.* 2015; 128(5): 939–942.
 45. Turek M., Drożdźiel A., Pyszniak K., Prucnal S., Mączka D. Production of Mo⁺ Beams Using an Arc Discharge Ion Source. *Acta Physica Polonica A* 2014; 125(6): 1388–1391.
 46. Turek M., Drożdźiel A., Pyszniak K., Filiks J., Prucnal S., Mączka D., Vaganov Yu., Węgierek P. Production of Molybdenum and Tantalum Ion Beams using CCl₂F₂, *Acta Physica Polonica A* 2017; 132(2): 283–287.
 47. Turek M., Drożdźiel A., Pyszniak K., Prucnal S. Production of rare earths ion beams in arc discharge ion source using their oxides, *Przegląd Elektrotechniczny* 2016; 92(8): 158–161.